Chinese Chemical Letters 35 (2024) 109182

Contents lists available at ScienceDirect

Chinese Chemical Letters

journal homepage: www.elsevier.com/locate/cclet

3D core-shell nanofibers framework and functional ceramic nanoparticles synergistically reinforced composite polymer electrolytes for high-performance all-solid-state lithium metal battery

Hengying Xiang[a,b], Nanping Deng[a,b,*], Lu Gao[a,b], Wen Yu[a,b], Bowen Cheng[a,b,*], Weimin Kang[a,b,*]

[a] State Key Laboratory of Separation Membranes and Membrane Processes, Tiangong University, Tianjin 300387, China
[b] School of Textile Science and Engineering, Tiangong University, Tianjin 300387, China

ARTICLE INFO

Article history:
Received 25 August 2023
Revised 17 September 2023
Accepted 6 October 2023
Available online 11 October 2023

Keywords:
Composite polymer electrolytes
Core-shell structured nanofiber
$Li_{6.4}La_3Zr_{1.4}Ta_{0.6}O_{12}$ ceramic nanoparticle
All-solid-state lithium metal batteries
Outstanding thermal stability and electrochemical performance

ABSTRACT

Satisfactory ionic conductivity, excellent mechanical stability, and high-temperature resistance are the prerequisites for the safe application of solid polymer electrolytes (SPEs) in all-solid-state lithium metal batteries (ASSLMBs). In this study, a novel poly(*m*-phenylene isophthalamide) (PMIA)-core/poly(ethylene oxide) (PEO)-shell nanofiber membrane and the functional $Li_{6.4}La_3Zr_{1.4}Ta_{0.6}O_{12}$ (LLZTO) ceramic nanoparticle are simultaneously introduced into the PEO-based SPEs to prepare composite polymer electrolytes (CPEs). The core PMIA layer of composite nanofibers can greatly improve the mechanical strength and thermal stability of the CPEs, while the shell PEO layer can provide the 3D continuous transport channels for lithium ions. In addition, the introduction of functional LLZTO nanoparticle not only reduces the crystallinity of PEO, but also promotes the dissociation of lithium salts and releases more Li^+ ions through its interaction with the Lewis acid-base of anions, thereby overall improving the transport of lithium ions. Consequently, the optimized CPEs present high ionic conductivity of 1.38×10^{-4} S/cm at 30 °C, significantly improved mechanical strength (8.5 MPa), remarkable thermal stability (without obvious shrinkage at 150 °C), and conspicuous Li dendrites blocking ability (>1800 h). The CPEs also both have good compatibility and cyclic stability with $LiFePO_4$ (>2000 cycles) and high-voltage $LiNi_{0.8}Mn_{0.1}Co_{0.1}O_2$ (NMC811) (>500 cycles) cathodes. In addition, even at low temperature (40 °C), the assembled $LiFePO_4$/CPEs/Li battery still can cycle stably. The novel design can provide an effective way to exploit high-performance solid-state electrolytes.

All-solid-state lithium metal batteries (ASSLMBs) using solid-state electrolytes (SSEs) can fundamentally change lithium deposition behavior and become one of the most effective solutions to resolve the problem of lithium metal anode in liquid lithium metal batteries [1–4]. Nowadays, SSEs, as one of the vital components of ASSLMBs, usually are mainly divided into solid polymer electrolytes (SPEs) and solid inorganic electrolytes (SIEs) [5,6]. SIEs usually have excellent ion conductivity and high Li^+ migration numbers [7]. However, due to the brittleness of SIEs [8], high processing cost, and poor interface contact, the implementation of practical applications still requires systematic research [9]. In comparison, SPEs usually have good mechanical flexibility and relatively tight adhesion with cell electrode, which can effectively adapt to the huge volume expansion of cell electrode during cycled battery, and has good interface compatibility between electrolyte and electrode [10–12]. Thus, it is expected to make a breakthrough and achieve wide application in portable electronic devices and electric vehicles [13].

In various SPEs, polyethylene oxide (PEO) has high permittivity, strong solvation ability of Li^+, and good flexibility of the molecular chain, which is one of the widely studied solid polymer electrolytes [14]. However, PEO is a semi-crystalline polymer with weak dynamic chain segments in the crystalline region, and pure PEO SPEs usually show low ionic conductivity below 10^{-6} S/cm at room temperature [15]. Besides its narrow electrochemical window (about 3.8 V), high interface impedance and unsatisfied mechanical properties also will result in the decline of battery cycle stability, bringing serious safety hazards and limiting its practical application for the fast development of lithium metal batteries [16].

* Corresponding authors.
E-mail addresses: dengnanping@tiangong.edu.cn (N. Deng), bowen15@tiangong.edu.cn (B. Cheng), kweimin@126.com (W. Kang).

https://doi.org/10.1016/j.cclet.2023.109182
1001-8417/

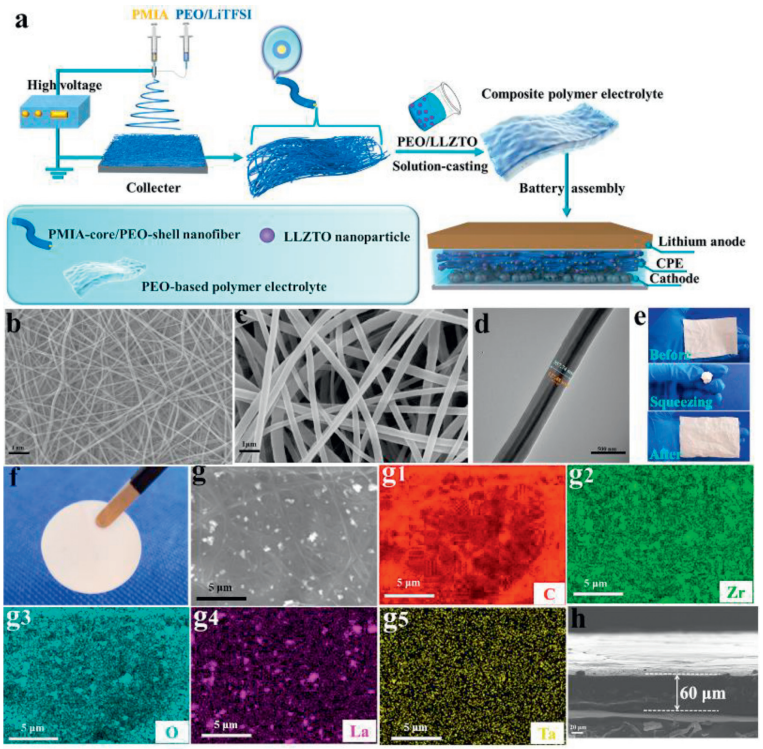

Fig. 1. (a) The schematic illustration for the preparation processes of the PMIA-core/PEO-shell nanofiber membrane, composite polymer electrolyte, and all-solid-state battery. (b) SEM images of PMIA nanofibers. (c) SEM images and (d) TEM image of C-PEO&PMIA nanofibers. (e) Digital photos of the C-PEO&PMIA nanofiber membranes squeezed into a cluster and before and after. (f) Digital photos of the PEO/LLZTO/C-PEO&PMIA CPEs. (g) The top-view SEM image of the PEO/6LLZTO/C-PEO&PMIA CPEs and EDS maps of the sample; (h) The cross-section SEM image of PEO/6LLZTO/C-PEO&PMIA CPEs.

To solve these intractable problems, many researchers have proposed various strategies such as blending [17], cross-linking [18], and the application of inorganic-organic composites to improve the performance of PEO-based polymer electrolytes [19]. Among them, adding active inorganic nanofillers containing Li atoms into the polymer matrix to prepare the organic/inorganic composite polymer electrolytes (CPEs) has been studied extensively [20–23], which can enhance electrical performances (*e.g.,* ionic conductivity, lithium-ion migration number) and provide the stable interfaces of single polymer phase. In addition, the introduction of a three-dimensional (3D) nanofiber membrane as a supporting framework in PEO polymer also can significantly improve the overall mechanical properties of solid electrolytes [24–26]. Electrospinning technology has been recognized as one of the simple methods for preparing uniform 3D nanofiber membranes [27,28]. In particular, if the 3D nanofiber membrane has excellent thermal stability, this also can ensure that the obtained PEO-SPEs still exhibit good cycling stability even at high temperatures and rates, significantly improving battery safety [29]. However, the introduction of non-lithium-ion conductor nanofibers limited the further improvement of ionic conductivity of the PEO-based polymer electrolytes to some extent. Therefore, a novel structural design is urgently needed to improve the mechanical properties, high-temperature resistance, and low ionic conductivity at room temperature of PEO-based CPEs.

In this work, coaxially spun PMIA-core/PEO-shell nanofiber membranes as the 3D supporting framework and $Li_{6.4}La_3Zr_{1.4}Ta_{0.6}O_{12}$ (LLZTO) nanoparticles as the functional nanofiller were simultaneously added into PEO/LiTFSI to obtain the optimized CPEs. Due to bulk compatibility, the PEO shell layer can promote the PEO-based polymer solution to be uniformly filled inside the nanofiber membrane. Meanwhile, it can also provide additional 3D lithium-ion transport channels for CPEs through the cooperation of complexation and decomplexation. In addition, the core layer PMIA, which is known for its exceptional mechanical strength, impressive thermal resistance, and excellent chemical stability, also can provide mechanical properties for the entire core-shell structure nanofiber, thereby improving the overall mechanical properties of the CPEs and ensuring the high-temperature resistance for electrolytes. The LLZTO nanoparticles, as ion-conductive inorganics, retain the general functions of inert fillers, such as reducing the crystallinity of PEO and promoting the dissociation of lithium salts through Lewis acid-base interactions. Meanwhile, they can also participate in the ion conduction process by forming additional lithium-ion transport pathways, thereby further improving the ion conductivity. As a result, the assembled Li/Li symmetrical cells with modified CPEs showed distinguished cyclic stability over 1800 h at 0.2 mA/cm^2 with a capacity of 0.2 mAh/cm^2. The $LiFePO_4$/CPEs/Li cells also displayed ultra-long cyclic stability over 2000 cycles at 1 C and 50 °C. Furthermore, the $LiFePO_4$/CPEs/Li also can cycle stably at 40 °C, and the Li/CPEs/$LiNi_{0.8}Mn_{0.1}Co_{0.1}O_2$ (NMC) batteries still have stable circulation and excellent Coulomb efficiency. The formed PMIA-core/PEO-shell nanofiber and LLZTO nanoparticles synergistically enhanced CPEs will undertake an encouraging preponderance to exploit the all-solid-state lithium metal batteries with excellent mechanical properties, outstanding thermal stability, and predominant electrochemical performance.

Fig. 1a displayed the preparation processes of PMIA-core/PEO-shell structure nanofiber membranes, flexible solid-state composite electrolytes, and all-solid-state lithium metal batteries. The details for the experimental section were fully introduced and presented in Supporting information. For simplicity, the prepared PMIA-core/PEO-shell structure nanofibers membrane was denoted as C-PEO&PMIA. The all-solid-state composite electrolyte was prepared by using the pure PEO and LiTFSI mixture solution; PEO, x wt% LLZTO nanoparticles and LiTFSI mixture solution; PMIA

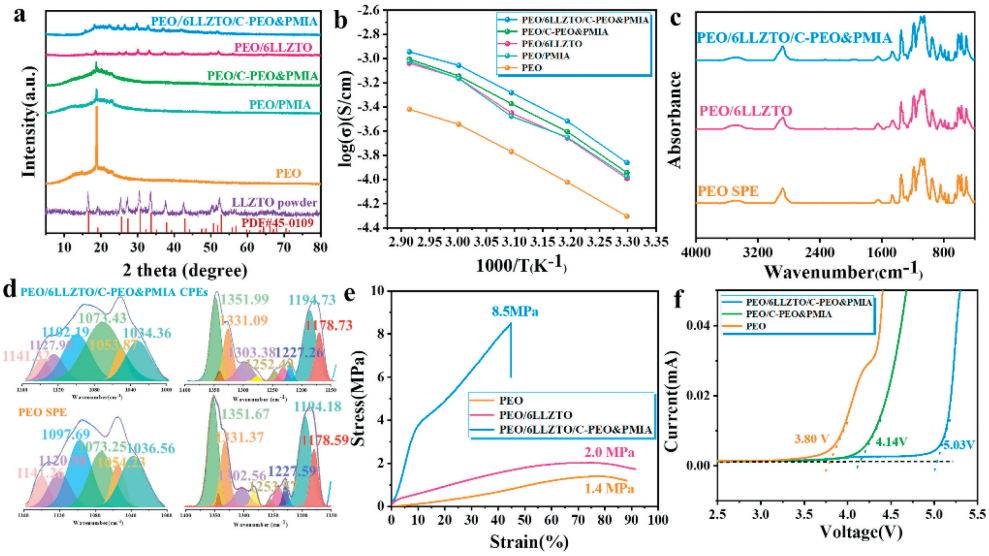

Fig. 2. (a) XRD patterns. (b) Arrhenius plots (temperature increased from 30 °C to 70 °C). FTIR spectra for PEO SPE and PEO/6LLZTO/C-PEO&PMIA CPE at (c) 4000–400 cm^{-1} and (d) 1160–1000 cm^{-1} and 1400–1150 cm^{-1}. (e) Stress-strain curves and (f) LSV curves of different electrolytes.

nanofiber membrane pouring PEO and LiTFSI mixture solution; C-PEO&PMIA nanofiber membrane pouring PEO and LiTFSI mixture solution; C-PEO&PMIA nanofiber membrane pouring PEO, 6 wt% LLZTO nanoparticles, and LiTFSI mixture solution were denoted as PEO, PEO/X LLZTO, PEO/PMIA, PEO/C-PEO&PMIA, PEO/6LLZTO/C-PEO&PMIA composite electrolytes, respectively.

Figs. 1b and c displayed the SEM image of the prepared PMIA and C-PEO&PMIA nanofibers. It can be clearly observed that the nanofibers cross each other to form reasonable pores and a 3D network structure. Besides, the TEM characterization technique was also used to characterize the successful preparation of core-shell nanofibers with PMIA as the core and PEO as a shell by the coaxial electrostatic spinning technology. As shown in Fig. 1d, the vivid core-shell structure of the inner PMIA was well encapsulated on the outer PEO, resulting in a graphically core-shell structure of the PEO&PMIA nanofibers. In addition, the diameter of PMIA as core-shell was about 127.48 nm, and the diameter of the whole core-shell nanofibers was about 357.74 nm. Fig. 1e showed the optical photographs of the prepared C-PEO&PMIA membrane, which exhibited a self-standing network-structured matrix. Besides, it can be folded like a nonwoven and completely recovered after rolling without any trace, indicating its superior mechanical and flexible properties at the same time. Subsequently, backfilling the C-PEO&PMIA membrane with a PEO-based mixture solution to obtain the PEO/LLZTO/C-PEO&PMIA CSEs for high-performance all-solid-state lithium metal batteries (Fig. 1f). Fig. 1g displayed the top-view SEM of the PEO/LLZTO/C-PEO&PMIA CPEs, which revealed a flat and homogeneous surface without pores and the LLZTO nanoparticle uniformly dispersed in the prepared CPEs. The corresponding EDS mapping images of carbon (C), zirconium (Zr), oxygen (O), lanthanum (La), and tantalum (Ta) manifested that the C-PEO&PMIA membrane and LLZTO nanoparticles were evenly dispersed in the CPEs, which was conducive to promoting the electrochemical performance of PEO/LLZTO/C-PEO&PMIA CPEs. According to the cross-section SEM image in Fig. 1h, the mechanically robust backbone of the C-PEO&PMIA membrane and the easily controlled application of the polymer precursor resulted in the thickness of the CPEs being about 60 μm.

Some studies have shown that the ionic transport mechanics of the amorphous region with activated chain segments is much faster than that of the crystalline phase [30]. The lower crystallinity of PEO meant that more polymer fragments can be involved in Li^+ transport, thus allowing SPE to achieve higher ionic conductivity. In order to further investigate the effect of the addition of LLZTO nanoparticles and the prepared PMIA and C-PEO&PMIA nanofiber membrane on the crystallinity of PEO, X-ray diffraction (XRD) was used to characterize the crystallinity. It can be observed clearly from Fig. 2a that after the introduction of PMIA and C-PEO&PMIA nanofibers, the related XRD diffraction peak of PEO was weakened significantly, stating that the crystallinity of PEO was greatly reduced. Moreover, in order to explore the optimal doping amount of LLZTO nanoparticles, the crystallization properties of electrolytes with packing mass fractions of 0 2, 4, 6, and 8 wt% were characterized (Fig. S1 in Supporting information). The results showed that the PEO-related XRD diffraction peak presented nonlinear changes with the increase of packing mass fraction in the range of 0–8 wt%. When the filler mass fraction was 6 wt%, the diffraction peak intensity of the electrolyte was the lowest among these samples. The introduction of LLZTO nanoparticles can reduce the crystallinity of PEO mainly due to its ability to destroy the aggregation structure of the polymer matrix, resulting in lower crystallinity [31]. However, excessive LLZTO nanoparticles also would lead to serious aggregation and reduce the free volume of polymer chain segments, which was not conducive to the fast transport of lithium ions [32]. When PEO-based electrolyte containing 6 wt% LLZTO nanoparticle was poured into the prepared C-PEO&PMIA nanofibers, the characteristic peak of PEO was also significantly weakened and the characteristic peak of LLZTO appeared, demonstrating that the LLZTO nanoparticle and C-PEO&PMIA nanofibers effectively promoted chain segment movement in the polymer electrolyte, thereby increasing the ionic conductivities of the composite electrolyte.

Fig. 2b and Fig. S2 (Supporting information) presented the ionic conductivity of the SPEs at different temperatures. Firstly, the influence of different LLZTO contents on the conductivity of electrolyte ions was investigated. As shown in Fig. S2, with the increased content of LLZTO nanoparticles, the ionic conductivities of CPEs initially increased and then decreased due to the agglomeration of excess LLZTO nanoparticles. The ionic conductivity arrived at a maximum when the addition of LLZTO nanoparticles was 8 wt%. Subsequently, the effects of PMIA and C-PEO&PMIA nanofibers membrane addition on the ionic conductivity for SPEs were also tested (Fig. 2b). The results showed that the ionic conductivities of SPEs containing PMIA or C-PEO&PMIA nanofibers membrane

were much higher than that of the prepared PEO SPE. Particularly, the PEO/C-PEO&PMIA CPEs exhibited superior ionic conductivities than PEO/PMIA CPEs. This is mainly because the shell PEO on the C-PEO&PMIA with core-shell structure can transport lithium ions along the nanofiber surface, which added the additional Li^+ transport channels for the composite electrolyte. Therefore, when 6 wt% LLZTO and C-PEO&PMIA nanofiber membrane were introduced simultaneously, the ionic conductivity of the electrolyte can be enhanced to 1.38×10^{-4} S/cm, which was much higher than that of pure PEO electrolyte (4.97×10^{-5} S/cm) at 30 °C. The contrasting results indicated that the simultaneous introduction of LLZTO nanoparticles and C-PEO&PMIA nanofibers membrane can significantly improve the Li^+ transport performance of the composite electrolyte.

The FTIR spectra of PEO SPE, PEO/6LLZTO CPEs, and PEO/6LLZTO/C-PEO&PMIA CPEs in the range of 4000–400 cm^{-1} were displayed in Fig. 2c. For better observing the small differences caused by the addition of LLZTO nanoparticle and C-PEO&PMIA nanofiber membrane to the PEO/LiTFSI matrix, the deconvoluted FTIR spectra in Fig. 2d presented the stretching vibrational modes of the C-O-C, -SO_2 and -CF_3 group in the frequency ranges 1160–1000 and 1400–1150 cm^{-1}, respectively. When compared to the C-O-C characteristic peaks of PEO electrolyte (1036.56, 1073.25, 1097.69, 1120.98, and 1141.26 cm^{-1}) [33], the prepared PEO/6LLZTO/C-PEO&PMIA CPEs have undergone a certain degree of deviation. The evolution of this C-O-C characteristic peak indicated a change in the chemical environment of the -EO group in the PEO can be obtained, further proving the interactions between C-O-C and LLZTO nanofillers and C-PEO&PMIA nanofiber [27]. Moreover, in the 1400–1150 cm^{-1} range, after introducing LLZTO nanoparticle and C-PEO&PMIA nanofiber membrane to the PEO SPE, the -SO_2 stretching corresponding to the peaks at 1331.37 and 1302.56 cm^{-1} shifted to 1331.37 and 1303.38 cm^{-1}, respectively. And the -CF_3 symmetric stretching corresponding to the peaks at 1253.57 and 1227.59 cm^{-1}, and the -CF_3 asymmetric stretching corresponding to the peaks at 1194.18 and 1178.59 cm^{-1} all shifted to varying degrees, respectively. These shifts -SO_2 and -CF_3 groups indicated that the LLZTO nanofillers and C-PEO&PMIA nanofiber membrane all had strong interactions with bis(trifluoromethane sulfonimide) ($TFSI^-$) anions, which effectively promoted the dissociation of LiTFSI and released more lithium ions [26].

Mechanical properties are one of the key properties of solid electrolytes in terms of alleviating the volume change of electrodes and inhibiting the penetration of lithium dendrites. The tensile stress-strain curves of various electrolytes were shown in Fig. 2e, and the test results revealed that the tensile strength of PEO/6LLZTO/C-PEO&PMIA CPEs can reach as high as 8.5 MPa, which was significantly higher than PEO/6LLZTO (2.0 MPa) CPEs and PEO (1.4 MPa) SPE. The satisfactory mechanical strength of the PEO/6LLZTO/C-PEO&PMIA CPEs was mainly due to the high-strength PMIA core layer nanofibers providing strong mechanical support for the CPEs, which can give the CPEs sufficient inhibition of lithium dendrite growth [34].

As one of the most intuitive parameters to measure the electrochemical stability of electrolytes, the electrochemical window, which is investigated by the linear sweep voltammetry (LSV) method, determines the voltage range of electrolytes and affects the upper limit of the energy density of the assembled lithium cells [35,36]. Fig. 2f displayed the LSV curves of various electrolytes. It can be seen that when the voltage of the PEO electrolyte was lower than 3.8 V, the oxidation current of the electrolyte was close to zero. But as the voltage continues to rise, the current increased significantly, indicating that the PEO electrolyte began to decompose around 3.8 V. In contrast, the decomposition voltage of PEO/C-PEO&PMIA CPEs and PEO/6wt% LLZTO CPEs can be significantly increased, which could reach 4.14 V and 4.75 V, respectively. It is worth mentioning that the decomposition voltage of PEO/6LLZTO/C-PEO&PMIA CPEs can reach as high as 5.03 V. These results indicate that the existence of core-shell C-PEO&PMIA composite nanofibers and LLZTO nanoparticles can effectively improve the electrochemical stability window of batteries, thus enhancing the safety performance of batteries. The main reasons for this phenomenon can be explained as follows: (1) The irreversible oxidation of $TFSI^-$ can significantly decrease the antioxidant stability of PEO. However, the strong Lewis acid-base interaction between the acid sites on the surface of LLZTO ceramic particles and salt anions also can effectively hinder the migration of $TFSI^-$, thereby significantly enhancing the electrochemical stability of the composite electrolyte [37]. (2) Higher ionic conductivity results in a decreased accumulation of Li^+ at the interfaces between the electrode and electrolyte, which effectively reduces the interfacial overpotential and greatly improves the compatibility between the electrode and electrolyte [18]. (3) The -NH in PMIA can form hydrogen bonding interactions with ether oxygen of PEO chains, which effectively improves the overall electrolyte's electrochemical stability window [38].

The EIS measurements were applied to test the SPEs/Li interface properties at 50 °C, and the result showed that the impedance of PEO/6LLZTO/C-PEO&PMIA CPEs had a smaller interfacial impedance than other SPEs (Fig. S3 in Supporting information), which was explained by the better interfacial contact between the cell electrodes and prepared electrolytes. To furth analyze the stability of the solid electrolytes to lithium metal, the constant discharge/charging voltage curves of different symmetric Li/SPEs/Li batteries were tested to examine the plating/stripping behavior and cycle stability of lithium. Firstly, the cyclic performance of various electrolytes at different current densities with an area capacity of 0.1 mAh/cm^2 at 50 °C was tested (Fig. 3a and Fig. S4 in Supporting information). The Li/PEO/Li symmetric battery appeared a short circuit at the current densities of 0.4 mA/cm^2 after about 25 h of cycling (Fig. S4a). In stark contrast, the Li/PEO/6LLZTO/C-PEO&PMIA/Li battery still retained lower polarization voltages and revealed a stable plating/peeling process even at high current densities of 0.8 mA/cm^2. And the Li/PEO/C-PEO&PMIA/Li battery started to fluctuate at a current density of 0.7 mA/cm^2 (Fig. S4b). The phenomenon indicated that lithium dendrites grow more easily with other electrolytes than that with PEO/6LLZTO/C-PEO&PMIA CPEs even at a low area capacity of 0.1 mAh/cm^2. Subsequently, the area capacity was increased to 0.2 mAh/cm^2 to further test the lithium plating/stripping performance of the assembled Li||Li cell using the prepared PEO/6LLZTO/C-PEO&PMIA CPEs under large area capacity. When compared with the Li/PEO/Li cell with short-circuited after only cycling for 87 h at 0.2 mAh/cm^2 (Fig. S5 in Supporting information), the prepared Li/PEO/6LLZTO/C-PEO&PMIA/Li cell can maintain a stable cycle as long as 1800 h (Fig. 3b). Furthermore, when the area density increased to 0.3 mAh/cm^2, the Li||Li cell assembled by PEO/6LLZTO/C-PEO&PMIA CPEs appeared no short-circuit even after 400 h with a small and smooth polarization, displaying an extraordinarily stable cycling performance (Fig. 3c). Specifically, if the prepared electrolyte lacks mechanical properties and ionic conductivity is poor, the lithium dendrites can simply form through the polymer matrixes. However, the inhibitory effect of prepared PEO/6LLZTO/C-PEO&PMIA CPEs on lithium dendrites mainly has two aspects: Firstly, the prepared core-shell nanofibers with high strength PMIA cores provided a strong supporting skeleton for the composite electrolytes to inhibit the growth of lithium dendrites. Secondly, the acidic sites on the surface of LLZTO nanoparticles can interact with $TFSI^-$ anions, leading to the weakening of the binding force of Li^+ and $TFSI^-$, thus significantly promoting the dissociation of LiTFSI, generating more Li^+ and improving the ionic conductivity, finally effectively inhibiting the formation of lithium dendrites.

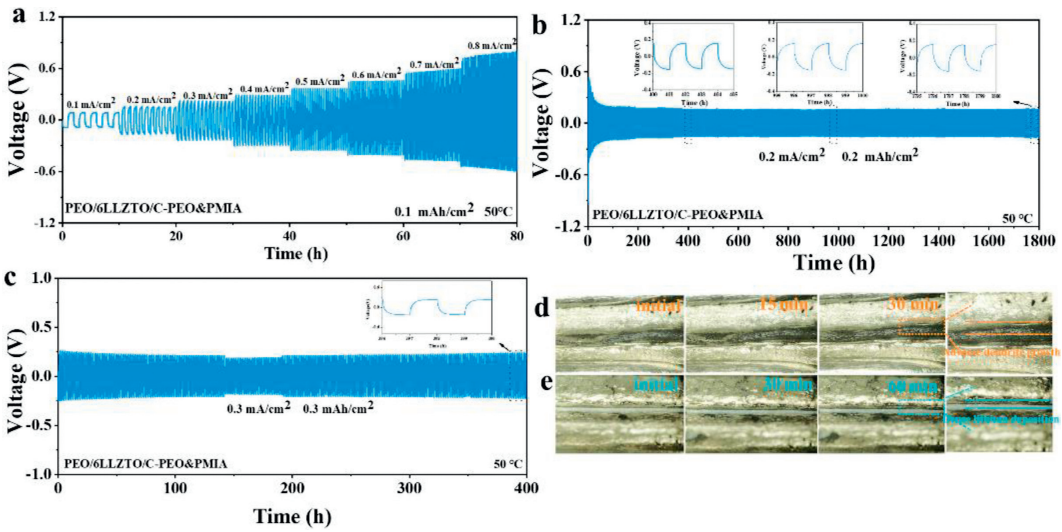

Fig. 3. The cycling performance of the Li/Li symmetric battery with PEO/6LLZTO/C-PEO&PMIA CPEs under 50 °C and different current densities at (a) 0.1 mAh/cm^2, (b) 0.2 mAh/cm^2 and (c) 0.3 mAh/cm^2. *In situ*, *in operando* observation of dendrite suppression at the cross-sectional interface between electrolyte and lithium metal of (d) Li|PEO|Li and (e) Li|PEO/6LLZTO/C-PEO&PMIA|Li symmetric cells. The cells continuously plated lithium at one interface testing at the current density of 0.2 mA/cm^2 at 50 °C.

For investigating the time required for lithium dendrites to pierce the electrolyte, the galvanostatic charging performance of the PEO electrolyte and PEO/6LLZTO/C-PEO&PMIA CPEs of the symmetric cell continuously plated lithium at one interface testing a current density of 0.2 mA/cm^2 at 50 °C were measured. It can be visualized from Fig. S6 (Supporting information) that the Li||Li cell using the PEO/6LLZTO/C-PEO&PMIA CPEs can retain as high as 29 h. In addition, by using an optical microscope *in-situ* device to track and observe the changes in the cross-section interface of Li|PEO/6LLZTO/C-PEO&PMIA|Li cells during the lithium deposition, it was found that the obtained PEO/6LLZTO/C-PEO&PMIA CSEs can effectively maintain a good interface, and dense and uniform lithium deposition (Fig. 3e). By contrast, the assembled Li||Li cell using the pure PEO electrolyte failed because of a short circuit after plating for just over 3 h, which was mainly due to the obvious lithium dendrite growth that began to appear after 0.5 h as shown in Fig. 3d. Those results once again highlighted the importance of the introduction of C-PEO&PMIA nanofiber membrane and LLZTO nanoparticle for significantly restraining the growth of Li dendrites.

Fig. S7 (Supporting information) presented surface morphology images of the symmetric Li/PEO/Li and Li/PEO/6LLZTO/C-PEO&PMIA/Li batteries were decomposed after the lithium plating/stripping at the current density of 0.2 mA/cm^2 for the area capacity of 0.2 mAh/cm^2 after 80 h. It was evident that the lithium surface of the Li/PEO/Li battery appeared massive loose and porous "dead Li" (Fig. S7a), which was mainly due to unstable and uneven Li^+ deposition. Marvelously, the Li surface from the prepared Li/PEO/6LLZTO/C-PEO&PMIA/Li battery was smooth and almost crack-free (Fig. S7b). The contrasted results proved that the obtained PEO/6LLZTO/C-PEO&PMIA CPEs had an obvious inhibitory effect on lithium dendrites and excellent cycling performance.

Fig. 4a have exhibited the specific discharge capacity changes of $LiFePO_4$/SPEs/Li at different rate. In order to more clearly compare the difference of various electrolytes at different rate, the specific picture was shown in Fig. S8 (Supporting information). The discharge capacity of the battery with PEO/6LLZTO/C-PEO&PMIA CPEs was 160.9, 159.6, 155.2, 155.2, and 140.3 mAh/g at rates of 0.2, 0.5, 1, and 2 C, respectively, which was higher than other electrolytes at all rate, and the difference was more pronounced at 2 C. When the current returns to 0.2 C, the discharge capacity of the battery can be restored to 160.8 mAh/g, exhibiting excellent rate performance. Moreover, when the rate returns to 0.5 C, the PEO/6LLZTO/C-PEO&PMIA CPEs assembled battery still can cycle stably for 500 cycles with 146.01 mAh/g discharge specific capacities and 99.9% average Coulombic efficiency (CE), showing just slight attenuation of discharge capacity. And the prepared PEO/C-PEO&PMIA CPEs assembled battery also kept the batteries stable cycle for 500 cycles with the 139.64 mAh/g discharge specific capacities of and 99.9% average CE. However, when compared with the Coulomb efficiency exaggerated fluctuation just appeared after 300 stable cycles of PEO/6LLZTO CPEs, the Coulombic efficiency of PEO SPEs dropped sharply after 150 cycles, displaying poor cycling stability. The long-term cycling performance of the $LiFePO_4$/PEO/6LLZTO/C-PEO&PMIA/Li battery at 1 C was further investigated and displayed in Fig. 4b. It can be seen that the $LiFePO_4$/Li batteries armed with the prepared PEO/6LLZTO/C-PEO&PMIA CPEs underwent a brief phase of rising capacity due to the improved surface contact between the CPEs and the electrodes [39,40]. After the ascent stage, the specific discharge capacity reached 142.8 mAh/g and can be maintained at 114.6 mAh/g after 2000 cycles with 99.9% average CE. Furthermore, Fig. S9 (Supporting information) showed the charging and discharging curves of the $LiFePO_4$/PEO/6LLZTO/C-PEO&PMIA/Li battery in different cycles, and the relatively stable curves indicated that the assembled battery had cycle stability. In contrast, the Coulomb efficiency of the $LiFePO_4$/PEO/Li battery decreased significantly just after 193 cycles (Fig. S10 in Supporting information). These contrasting results were mainly due to the continuous lithium-ion transport channels formed by the PEO shell layer wrapped in the outer layer of PMIA, which greatly promoted the transport of lithium ions. The inner shell PMIA fiber provided excellent mechanical strength for the composite electrolyte, making it effectively resistant to lithium dendrites and ensuring stable cycling of the battery. In addition, the PEO electrolytes can be uniformly filled within the nanofiber membrane due to the bulk compatibility, which facilitated the transport of lithium ions within the CPEs. And the applied LLZTO nanoparticles also can effectively promote the dissociation of lithium salts, resulting in excellent ion conductivity of the composite electrolyte.

The cycling performance of PEO/6LLZTO/C-PEO&PMIA CPEs at lower temperatures (40 °C) was also tested (Fig. 4c), which maintained a stable discharge capacity of 128.7 mAh/g after 200 cycles. To demonstrate the practical feasibility of the CPEs, the

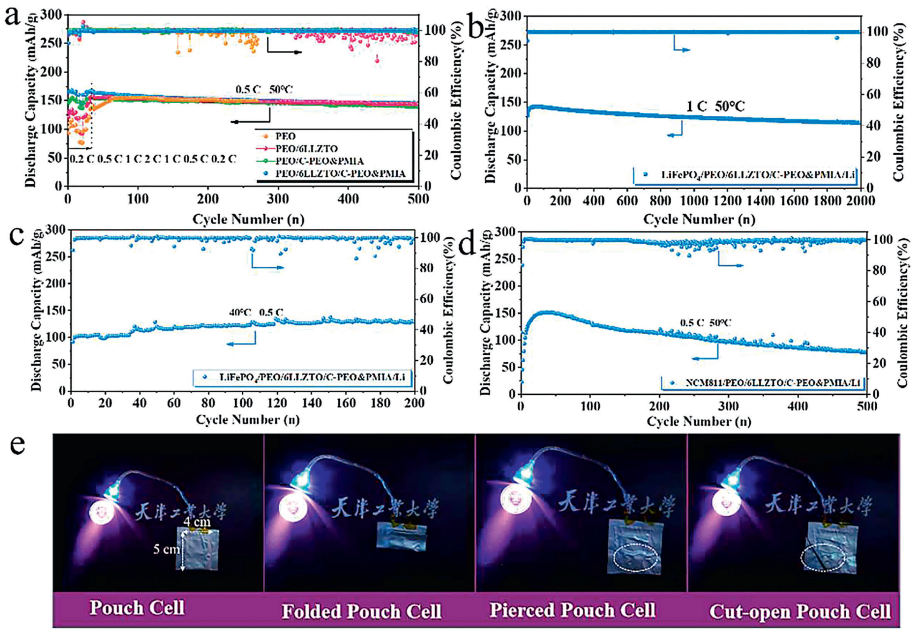

Fig. 4. (a) Cycling performance of different cells at various rates. Cycling performance of $LiFePO_4$/PEO/6LLZTO/C-PEO&PMIA/Li at (b) 1 C and 50 °C and (c) 0.5 C and 40 °C. (d) Cycling performance of NMC811/PEO/6LLZTO/C-PEO&PMIA/Li at 0.5 C and 50 °C. (e) The reliability and safety of the $LiFePO_4$/PEO/6LLZTO/C-PEO&PMIA/Li pouch cell under normal, folding, punching, and cutting conditions.

PEO/6LLZTO/C-PEO&PMIA pouch cells were also assembled. Besides, the ability of the pouch cell to function properly in extreme conditions is key to putting it to practical use [41]. Fig. 4e shows the successful operation of the ultra-thin PEO/6LLZTO/C-PEO&PMIA pouch cell, measuring 4 cm×5 cm, in powering a light bulb at room temperature. Remarkably, the bulb remained illuminated even when the cell was subjected to folding, piercing, and cutting. The remarkable safety performance can be attributed to the presence of PMIA-core/PEO-shell nanofiber, which can significantly contribute to the overall safety of ASSLMBs.

To evaluate the compatibility between the composite electrolyte and the high-voltage cathode, the applied $LiNi_{0.8}Mn_{0.1}Co_{0.1}O_2$ (NMC)/PEO/6LLZTO/C-PEO&PMIA/Li all-solid-state battery was also assembled. As shown in Fig. 4d, the NMC/Li battery assembled by PEO/6LLZTO/C-PEO&PMIA CPEs still had a discharge capacity of 78.2 mAh/g even after 500 cycles at 0.5 C and 50 °C, which proved that it has good high-voltage cycle stability. Fig. S11 (Supporting information) displayed the charge/discharge curves of the NMC/PEO/6LLZTO/C-PEO&PMIA/Li battery under 0.5 C and 50 °C after different cycles, from which it can be seen that the battery always had a smooth charging and discharging platform, indicating the long-term effectiveness of the battery interfaces. The excellent cycle stability can be attributed to the good interfaces between the composite electrolyte and the high-voltage cathode, its high electrochemical stability window, and excellent ionic conductivity.

Compared with the traditional liquid electrolyte, solid electrolyte has higher safety, stability, and power density, which can significantly improve the cycle life and energy density of the battery. However, solid electrolytes also have some problems, the most serious of which may be the problem of thermal stability. The thermal stability of solid electrolyte refers to its changing degree of physical and chemical properties and thermal decomposition threshold at high temperatures. In the battery charging and discharging processes, the electrolyte will be affected by high temperature. If its thermal stability is not good, this will be easy to lead to the reaction inside the battery being out of control, and even explosion, fire, and other accidents. Therefore, for solid electrolytes, it also is very important to ensure that they have good thermal stability. Fig. 5a presented the dimensional stability comparison test of pure PEO, PEO/6LLZTO, and PEO/6LLZTO/C-PEO&PMIA solid electrolyte after heating at 30, 60, 90, 120 and 150 °C for 1 h, respectively. It can be seen that the PEO and PEO/6LLZTO solid electrolytes shrank significantly as the temperature gradually increased. The solid electrolytes containing the prepared core-shell nanofiber membrane did not have major morphological changes even at 150 °C. The phenomenon illustrated that the PMIA introduced into the core layer provided excellent thermal stability for the composite solid electrolyte, which can meet the needs of high-temperature conditions, greatly improving the safety performance of all-solid lithium metal batteries. Fig. 5b exhibited the TG curve tested in the air atmosphere to analyze the thermal decomposition process of different SPEs. It can be seen that the first weight loss below 200 °C was mainly due to the volatilization of residual solvents. While the second weight loss above 400 °C can be attributed to the decomposition of PEO [42]. The results emphasized that the prepared composite electrolyte had good thermal stability and was conducive to its practical application.

Finally, visualization experiments were conducted on four experimental samples of combustion. Fig. 5c presented a combination of screenshots of various electrolytes at different time points. It can be seen that when a high-temperature flame approached, the PEO solid electrolyte ignited rapidly within 1 s and continued to burn, accompanied by a drop in liquid droplets. This was a typical phenomenon of polymer combustion, which ultimately burned completely within 6 s. However, the composite electrolytes containing PMIA nanofibers exhibited self-extinguishing behavior, with only a small amount of carbonized areas retained at their edges, indicating that the introduction of PMIA with excellent thermal stability results in better flame retardancy of the obtained composite electrolyte. The conclusion indicated that PEO/6LLZTO/C-PEO&PMIA was a flame retardant and environmentally friendly composite electrolyte. The prepared CPEs also had good mechanical strength and well thermal stability, which can effectively prevent short-circuit problems caused by electrolyte deformation. At the same time, a wider electrochemical window also meant that there would be opportunities to adapt to more cathode materials

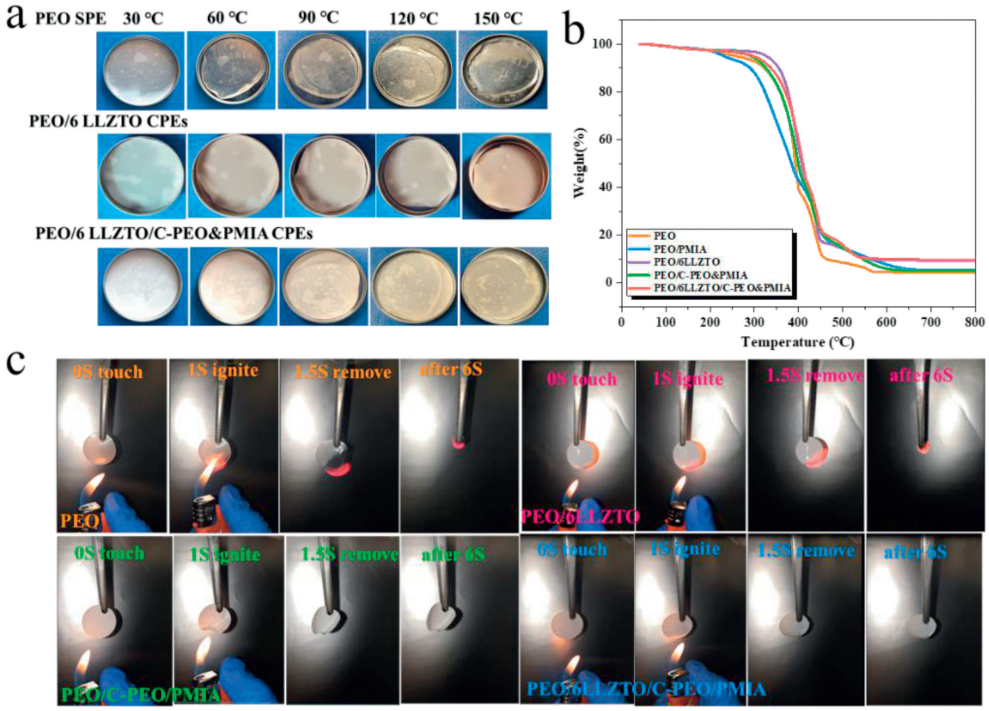

Fig. 5. (a) Optical images of various solid electrolytes treated at different temperatures for 1 h. (b) TG measurements of various samples. (c) Photo images of flame test on different electrolytes.

in the future. Based on the premise that PEO/6LLZTO/C-PEO&PMIA CPEs have flame retardancy, this is an effective way to improve the performance of batteries at high temperatures and also an important guarantee for its future applications.

In summary, the novel PMIA-core/PEO-shell nanofiber membranes were successfully prepared by the facile coaxial electrospinning technology and then backfilled with PEO/LiTFSI/LLZTO by solution casting way. The evenly dispersed LLZTO nanoparticles with fast lithium-ion conductors in the composite electrolyte not only effectively inhibited the crystallization of PEO polymer, but also stimulated the dissociation of lithium salts through Lewis acid-base interaction, enhancing the rapid migration of lithium ions. Furthermore, the prepared PMIA-core/PEO-shell nanofiber not only established 3D Li^+ transport channels, but also can serve as strong framework support to improve the mechanical properties of optimized CPEs, thereby effectively inhibiting the growth of lithium dendrites. Therefore, the PEO/6LLZTO/C-PEO&PMIA CPEs demonstrated outstanding rate performance and cycling stability at 50 °C, which can also cycle steadily at 40 °C. This study provides an effective technique for the preparation of CPEs with good electrochemical stability, high-temperature resistance, and excellent safety.

Declaration of competing interest

The authors declare that they have no known competing financial interests or personal relationships that could have appeared to influence the work reported in this paper.

Acknowledgments

This work was supported by the National Natural Science Foundation of China (Nos. 52203066, 51973157, 61904123), the Tianjin Natural Science Foundation (No. 18JCQNJC02900), National Innovation and Entrepreneurship Training Program for College students (No. 202310058007), Tianjin Municipal College Students' Innovation and Entrepreneurship Training Program (No. 202310058088), Science & Technology Development Fund of Tianjin Education Commission for Higher Education (No. 2018KJ196), and State Key Laboratory of Membrane and Membrane Separation, Tiangong University.

Supplementary materials

Supplementary material associated with this article can be found, in the online version, at doi:10.1016/j.cclet.2023.109182.

References

[1] Q. Song, Y. Zhang, J. Liang, et al., Chin. Chem. Lett. 35 (2024) 108797.
[2] J. Kang, N. Deng, Y. Liu, et al., Energy Storage Mater. 52 (2022) 130–160.
[3] C. Yang, K. Fu, Y. Zhang, et al., Adv. Mater. 29 (2017) 1701169.
[4] J.K. Hu, H. Yuan, S.J. Yang, et al., J. Energy Chem. 71 (2022) 612–618.
[5] H. Xu, J. Zhang, H. Zhang, et al., Adv. Energy Mater. 13 (2023) 2204411.
[6] H. Gao, N.S. Grundish, Y. Zhao, et al., Energy Mater. Adv. 2021 (2021) 1932952.
[7] H. Zhang, Z. Yu, J. Cheng, et al., Chin. Chem. Lett. 34 (2023) 108228.
[8] C. Li, R. Li, K. Liu, et al., Interdiscip. Mater. 1 (2022) 396–416.
[9] H.W. Kim, J. Han, Y.J. Lim, et al., Adv. Funct. Mater. 31 (2021) 2002008.
[10] Y.L. Liao, J.K. Hu, Z.H. Fu, et al., J. Energy Chem. 80 (2023) 458–465.
[11] L. Wu, Y. Wang, X. Guo, et al., SusMat 2 (2022) 264–292.
[12] X. Shen, X.Q. Zhang, F. Ding, et al., Energy Mater. Adv. 2021 (2021) 1205324.
[13] S. Tang, W. Guo, Y. Fu, Adv. Energy Mater. 11 (2021) 2000802.
[14] P. Chen, X. Liu, S. Wang, et al., ACS Appl. Mater. Interfaces 11 (2019) 43146–43155.
[15] L.Z. Fan, H. He, C.W. Nan, Nat. Rev. Mater. 6 (2021) 1003–1019.
[16] Z. Zhang, Q. Zhang, C. Ren, et al., J. Mater. Chem. A 4 (2016) 15823–15828.
[17] L. Gao, J. Li, J. Ju, et al., Compos. Sci. Technol. 200 (2020) 108408.
[18] X. Zheng, J. Wei, W. Lin, et al., ACS Appl. Mater. Interfaces 14 (2022) 5346–5354.
[19] G. Wang, Y. Liang, H. Liu, et al., Interdiscip. Mater. 1 (2022) 434–444.
[20] Q. Yu, K. Jiang, C. Yu, et al., Chin. Chem. Lett. 32 (2021) 2659–2678.
[21] Y. Na, Z. Chen, Z. Xu, et al., Chin. Chem. Lett. 33 (2022) 4037–4042.
[22] Y. Zheng, Y. Yao, J. Ou, et al., Chem. Soc. Rev. 49 (2020) 8790–8839.
[23] T.T. Vu, H.J. Cheon, S.Y. Shin, et al., Energy Storage Mater. 61 (2023) 102876.
[24] F. Zhang, Y. Si, J. Yu, et al., Chem. Eng. J. 456 (2023) 140989.
[25] Y. Zhao, J. Yan, J. Yu, et al., ACS Nano 16 (2022) 17891–17910.
[26] L. Gao, J. Li, J. Ju, et al., Chem. Eng. J. 389 (2020) 124478.
[27] Q. Li, X. Sun, D. Cao, et al., Electrochem. Energy Rev. 5 (2022) 18.
[28] H. Chen, M. Li, C. Li, et al., Chin. Chem. Lett. 33 (2022) 141–152.
[29] Y. Ma, J. Wan, Y. Yang, et al., Adv. Energy Mater. 2022 (2022) 2103720.
[30] W.A. Henderson, N.R. Brooks, V.G. Young, J. Am. Chem. Soc. 125 (2003) 12098–12099.

[31] C. Shen, Y. Huang, J. Yang, et al., Energy Storage Mater. 39 (2021) 271–277.
[32] L. Chen, Y. Li, S.P. Li, et al., Nano Energy 46 (2018) 176–184.
[33] X.L. Zhang, F.Y. Shen, X. Long, et al., Energy Storage Mater. 52 (2022) 201–209.
[34] D. Li, L. Chen, T. Wang, et al., ACS Appl. Mater. Interfaces 10 (2018) 7069–7078.
[35] L. Gao, J. Li, B. Sarmad, et al., Nanoscale 12 (2020) 14279–14289.
[36] B. Streipert, L. Stolz, G. Homann, et al., ChemSusChem 13 (2020) 5301–5307.
[37] L. Yue, J. Ma, J. Zhang, et al., Energy Storage Mater. 5 (2016) 139–164.
[38] X. Chen, X. Li, L. Luo, et al., Adv. Energy Mater. (2023) 2301230.
[39] J.L. Ma, F.L. Meng, Y. Yu, et al., Nat. Chem. 11 (2019) 64–70.
[40] C. Yan, P. Zhu, H. Jia, et al., Energy Storage Mater. 26 (2020) 448–456.
[41] X.Q. Xu, X.B. Cheng, F.N. Jiang, et al., SusMat 2 (2022) 435–444.
[42] J. Hu, W. Wang, B. Zhou, et al., J. Membr. Sci. 575 (2019) 200–208.